Negative refraction of acoustic waves in two-dimensional sonic crystals

Liang Feng,[1] Xiao-Ping Liu,[1] Yan-Bin Chen,[1] Zhi-Peng Huang,[1] Yi-Wei Mao,[2] Yan-Feng Chen,[1,*] Jian Zi,[3] and Yong-Yuan Zhu[1]

[1]*National Laboratory of Solid State Microstructures, Nanjing University, Nanjing 210093, People's Republic of China*

[2]*Institute of Acoustics, Nanjing University, Nanjing 210093, People's Republic of China*

[3]*Surface Physics Laboratory, Fudan University, Shanghai 200433, People's Republic of China*

(Received 19 July 2004; revised manuscript received 21 January 2005; published 18 July 2005)

Negative refractions of acoustic waves in a two-dimensional (2D) sonic crystal were studied both experimentally and theoretically. By calculating the acoustic band structure and equifrequency surfaces, we theoretically analyzed the acoustic single-beam negative refraction in the first band operating in the ultrasonic regime. A 2D square sonic crystal was constructed with 2.0-mm-diam steel cylinders arranged as square arrays of 2.5 mm lattice constant. A scanning transmission measurement of spatial distribution was carried out to establish the acoustic refraction of a single Gaussian beam. It was demonstrated that the negative refraction is strongly dependent on both frequencies and incident angles, which shows great potential in acoustic devices.

DOI: 10.1103/PhysRevB.72.033108 PACS number(s): 43.35.+d, 63.20.−e

Negative refractions of electromagnetic (EM) waves were theoretically predicted in the left-handed material (LHM) by Veselago in 1968.[1] Due to its unique physical properties and potential applications, the study of negative refractions has been a hot focus of interest recently. There are two approaches to realize EM negative refraction, plasmon resonances in metamaterials[2–7] and multiple scatterings in photonic crystals (PCs).[8–13]

In metamaterials, plasmon resonances of two-dimensional (2D) arrays consisting of split-ring resonators and wires can be used to fabricate LHM, which as a whole has both negative effective permittivity and negative permeability in a certain microwave range.[5–7] Based on the above prediction, a flat LHM slab with $\varepsilon=-1$ and $\mu=-1$ was proposed by Pendry to realize a so-called perfect lens[14] in which both propagating and evanescent waves contribute to the image, and some relevant phenomena have been experimentally demonstrated.[15]

In photonic crystals, the existence of negative refractions is due to intense multiple scatterings near the Brillouin-zone boundaries.[8–13] Similar to the perfect lens in LHM, negative refractions in PCs could also result in a flat lens, called superlens, whereby it is possible to obtain the transmission amplitude for evanescent waves to produce a real image.[12,13,16] This phenomenon was observed experimentally in the microwave and infrared ranges,[17,18] showing great promise in photoelectronic applications.

Recently, negative refractions were also realized in other kinds of classical waves. Liquid surface waves in a periodic structure of copper cylinders were characterized by band structures resulted from multiple scatterings,[19] leading to negative refraction and a superlensing effect.[20] The same phenomena have been realized recently for acoustic waves.[21,22] In this paper, we studied, both experimentally and theoretically, the dependence of the negative refraction of acoustic waves on frequencies and incident angles in a 2D sonic crystal (SC).

In SCs, Lamé coefficients $\lambda(r)$, $\mu(r)$, and the (mass) density $\rho(r)$ are modulated periodically and acoustic waves can be described in terms of a band structure, as in the case of electrons and photons.[23–25] The wave equation can be written as[26]

$$\frac{\partial^2 u^i}{\partial^2 t}=\frac{1}{\rho}\left\{\frac{\partial}{\partial x_i}\left(\lambda\frac{\partial u^l}{\partial x_l}\right)+\frac{\partial}{\partial x_l}\left[\mu\left(\frac{\partial u^i}{\partial x_l}+\frac{\partial u^l}{\partial x_i}\right)\right]\right\}\quad i,l=1,2,3, \tag{1}$$

where u^i $(i=1,2,3)$ are the Cartesian components of the displacement vector $u(r)$, and x^l $(l=1,2,3)$ are the Cartesian components of the position vector.

In the present experiment, in order to manufacture a 2D SC, an aluminum plate was drilled to be a square array of holes with the radius of 1.0 mm and the lattice constant of 2.5 mm. In the lateral direction of the plate, holes were arranged in the (1, 1) direction with 79 layers and in the perpendicular direction with 27 layers. The 2D SC was constructed by inserting 250-mm-long steel cylinder rods with the radius of 1.0 mm into the periodically drilled plate. Hence, our SC was a 2D square SC with steel cylinders in air background $[\rho_{steel}=7800\ \mathrm{kg/m^3}$, $\rho_{air}=1.21\ \mathrm{kg/m^3}$, $c_{steel}=6100\ \mathrm{m/s}$, $c_{air}=334.5\ \mathrm{m/s}$ (sound velocity in air at 0 °C)], in which the lattice constant is $a=2.5$ mm and the radius of cylinders is $R=1.0$ mm, resulting in a filling fraction $\pi R^2/a^2$ of approximately 50%.

For the SC consisting of steel and air, only the longitudinal waves are allowed. Then Eq. (1) could be simplified as follows:[27]

$$\frac{1}{\lambda}\frac{\partial^2 u}{\partial^2 t}=\nabla\cdot\left(\frac{\nabla u}{\rho}\right). \tag{2}$$

By using the plane-wave expansion (PWE) method[28] and applying the Bloch theorem, Eq. (2) could yield the eigenvalue equation as

$$\sum_{\vec{G}'}\left[\omega^2\lambda^{-1}_{\vec{G}-\vec{G}'}-\rho^{-1}_{\vec{G}-\vec{G}'}(\vec{K}+\vec{G})\cdot(\vec{K}+\vec{G}')\right]u_{\vec{G}'}=0, \tag{3}$$

where $\vec{K}$ is restricted within the first Brillouin zone and $\vec{G}$ is the reciprocal vector. By using 289 plane waves, the band structure is calculated as shown in Fig. 1(a). With more plane waves, such as 625 plane waves, the calculated band structure in the first and second bands is the same too. Based on this band structure, the acoustic equifrequency surface (EFS)

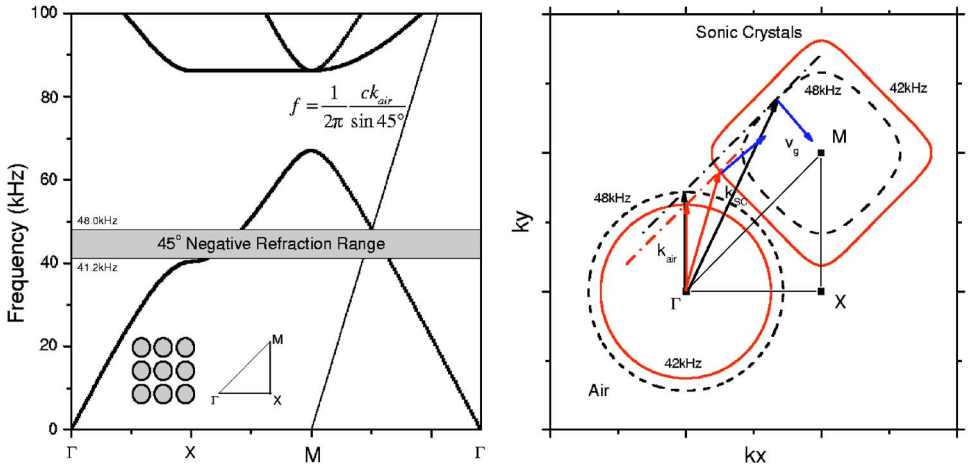

FIG. 1. (Color online) Theoretical demonstration of the acoustic negative refraction. (a) is the band structure of the SC. The shading region denotes the negative refractive frequency range from 41.2 to 48.0 kHz with the incident beam making 45° with Γ–M direction. (b) is the EFS in k space of the air and SC at 42 kHz (solid) and 48 kHz (dashed), respectively; k_{SC} and v_g are the wave vector and group velocity in the SC, respectively.

[Fig. 1(b)] is constructed for the acoustic waves propagating from air to the SC with the interface normal along the (1, 1) direction ($\Gamma - M$ in k space). It is well known, for the square lattice, that the lowest band has $k \cdot \partial\omega/\partial k \geqslant 0$ everywhere within the first Brillouin zone. In other words, the group velocity is never opposite to the phase velocity. From Fig. 1(b) we can see that for frequencies that correspond to all-convex contours, the group velocity points to the M point. In this case, the incidence and refraction will stand on the same side of the interface normal, resulting in the acoustic negative refraction. Otherwise, when the EFS is concave around the M point, the group velocity $\partial\omega/\partial k$ points away from the M point, leading to the positive refraction.

To verify the analysis of the refraction of acoustic waves, the fabricated SC was arranged with 27 layers in the propagating direction and 79 layers in the lateral direction. A scanning transmission measurement of spatial distributions covering frequencies from 37 to 44 kHz was carried out by various incident angles. In our experiment (Fig. 2), the SC with the interface of $\Gamma - M$ direction [(1,1) in real space] was placed between two transducers (Airmar AR41, USA), one as an emitter and the other as a receiver. A continuous acoustic incident Gaussian beam from the emitting transducer was generated by a function generator (Agilent 33120A, USA). To eliminate the angular divergence and obtain a good Gaussian shape, we carried out a 100-mm-long, 15-mm-thick sponge loop with an inner radius of 15 mm as an absorbing waveguide between the SC and the emitting transducer. So a good Gaussian beam could be obtained by absorbing acoustic waves with large angles. We measured the amplitudes with both the absorber and no absorber. The results (the inset of Fig. 2) showed that the width of the half peak decreased 1/2 times when waves propagated through the absorber, indicating a good Gaussian shape with angular divergence less than 7°. The receiving transducer was mounted on a goniometer that ran along the lateral direction

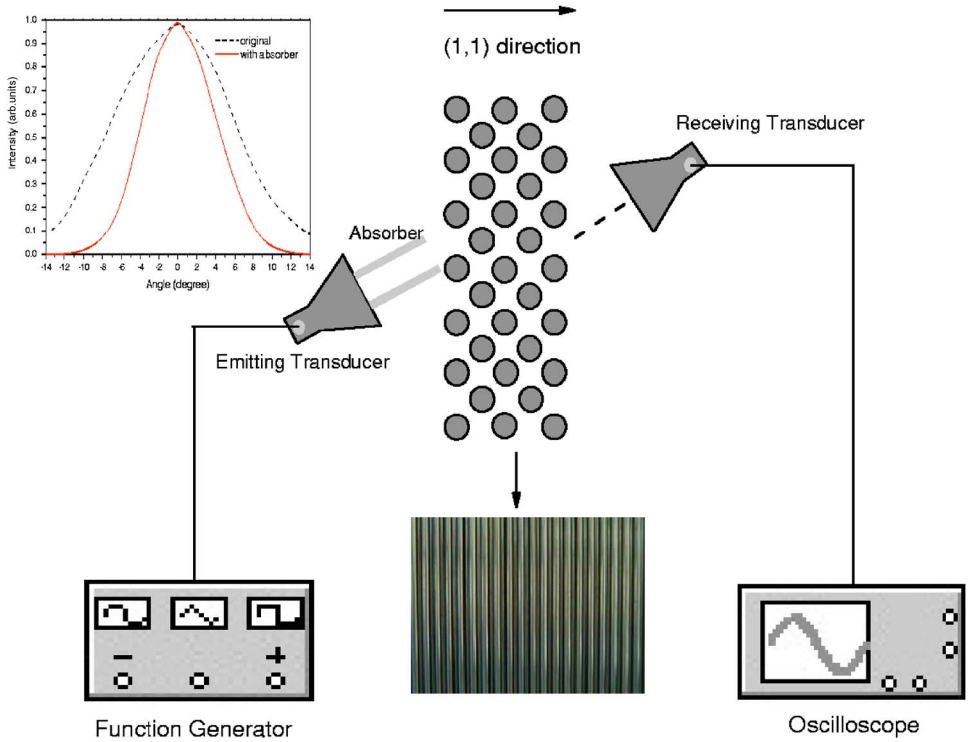

FIG. 2. (Color online) Schematic of the experimental setup used to measure the transmission of ultrasonic wave in a SC, consisting of two transducers, a flat rectangular slab of steel cylinders, a function generator, and an oscilloscope. The SC, the rectangular slab of steel cylinders shown as the middle-bottom inset, is placed between two transducers and the left-top inset shows measurements of the amplitude comparisons with the absorber (solid) to without the absorber (dashed).

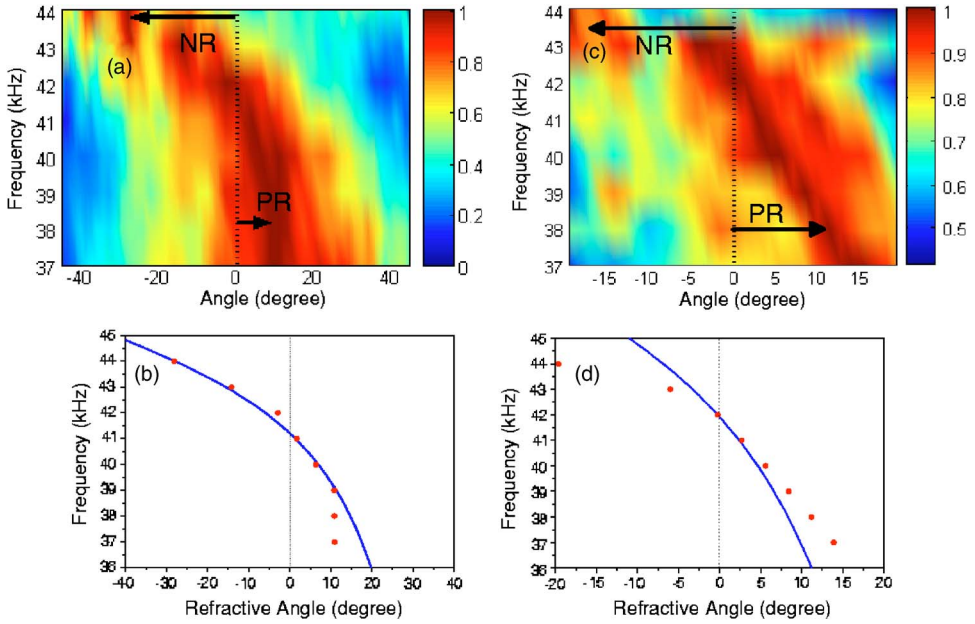

FIG. 3. (Color online) The dependence of negative refractions on frequencies. (a) and (c) are the average acoustic transmission intensity vs frequencies (kHz) and angles for the SC with the incident angle of (a) 45° and (c) 30°. The refraction was established as the negative refraction (NR) or the positive refraction (PR) if the maximum transmission intensity is detected at the left or right side of the surface normal, respectively. The average intensity scale varies from 0 to 1. (b) and (d) are comparisons of experimental measurements (dots) and theoretical simulations (lines) of refractive angles vs frequencies with the incident angle of 45° and 30°.

parallel with the SC interface. The detector was positioned at 10 cm away from the refraction surface to eliminate near field effects. The transmission signal was acquired by a digital sampling oscilloscope with a temporal resolution of 2.5 ns. The refraction was considered negative (positive) if the emerging beam is detected at the same (different) side of the surface normal as the incident beam.

The dependence of refractions on frequencies is shown in Fig. 3 with a,b for the incident angle of 45° and c,d for the case of 30°, respectively. In the experiment, both the emitter and receiver were oriented to the same angle of 45° or 30° with respect to the surface normal. For a better contrast, the data are represented in terms of the average transmission intensity. For the frequencies below 41 kHz shown in Fig. 3(a), the center of the outgoing Gaussian beam is shifted to the right and the positive refraction is observed. Above 42 kHz, the beam center shifts to the left, corresponding to the negative refraction. Notice that the refractive angle is dependent on frequencies. By employing PWE methods with 289 plane waves, the refractive direction with the frequency was calculated as shown in Fig. 3(b). The negative refraction for the incident angle of 45° starts to appear at the frequency of 41.2 kHz, which is very close to the experimental measurements with the refractive angle of 1.7° at 41 kHz and −2.9° at 42 kHz, respectively. Above the negative-refraction-starting frequency of 41.2 kHz, the higher the frequency, the larger the negative refractive angle. In the range of scanning frequencies from 37 to 44 kHz, the negative refractive angle reached its maximum of theoretical −27.8° and experimental −28.0° at 44 kHz. The experimental measurements and theoretical calculations for the incident angle of 30° are shown in Figs. 3(c) and 3(d). The negative-refraction-starting frequency was theoretically calculated at 41.9 kHz, which agrees very well with our experimental results by 2.1° at 41 kHz and −0.2° at 42 kHz. Meanwhile, at the same frequency, the negative refractive angle for the incident angle of 45° is always greater than that with 30°.

In the experiment, results for 30° incidence are not as good as those for 45°, which is resulted from the angular divergence and the big size (5-cm-diam) of the receiving transducer. Both characters of the receiver result in a low resolution to the refraction beam. For a bigger incident angle, the refractive angle is greater so that the refraction could be easily resolved and the receiver's resolution is high enough to get accurate measurements. While for a smaller incident angle, the refractive angle is also smaller, for example, the maximum around 7° at 44 kHz for 30° incidence, so the low resolution of the receiver leads to the bigger aberrance. To reduce this inaccuracy, a perfect Gaussian beam is needed, however, unfortunately it is quite difficult to realize in the regime of several tens of kHz.

These observations could be well understood by examining the acoustic anisotropic EFS [Fig. 1(b)]. The corresponding acoustic EFS and its curvature determine the direction of acoustic refraction in SCs. With the increase of frequencies, the SC's EFSs are easier to convex around the M point so that negative refractions will occur at higher frequencies. The higher operating frequency results in the smaller EFS around the M point; and the curvature of the corresponding point at the EFS is greater, which leads to a bigger negative refractive angle. When the EFS is small enough, however, there exists a stopping frequency because the total internal reflection occurs at the directional band gap for a single acoustic beam, which could be calculated by using a similar method that determines the upper limit of all angle negative refraction (AANR).[12] The shading region in Fig. 1(a) denotes the negative refractive frequency range from 41.2 to 48.0 kHz with the incident beam making 45° with $\Gamma-M$ direction. Differed from $f=ck_{air}/2\pi$ calculated in AANR, we calculate the dispersion line by $f=(1/2\pi)ck_{air}/\sin 45° = \sqrt{2}ck_{air}/2\pi$, whose intersection with the band structure indicates the frequency 48.0 kHz with the maximum negative refractive angle of −90°.

The negative refraction is also strongly dependent on the incident angles of the acoustic beam. The anisotropy of the SC's EFSs could also be used to describe relations between

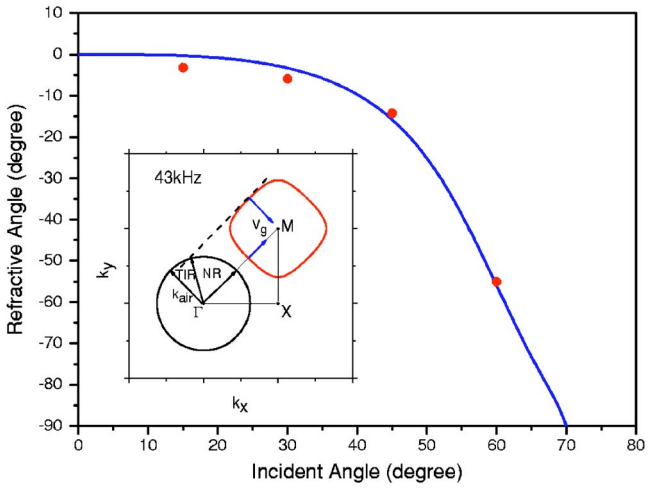

FIG. 4. (Color online) Comparison of measured (dots) and calculated (lines) angles of refractions versus angles of incidences at 43 kHz. The inset is the EFSs at 43 kHz, in which NR and TIR indicate the incident angles with the negative refraction and total internal reflection, respectively.

negative refractions and incident angles at a constant frequency. To demonstrate this effect, the angles of refraction are theoretically calculated by the PWE method with 289 plane waves and experimentally measured with a variety of incident angles at 43 kHz as depicted in Fig. 4. We got good agreements between theoretical calculations and experiment measurements, for example, the refractive angle theoretically −15.6° and experimentally −14.2° with the incident angle of 45°, and theoretically −55.9° and experimentally −55.0° with the incident angle of 60°, respectively. If the angle of incidences is bigger than 70°, there exists the directional band gap; then the acoustic wave will experience total internal reflection and no refraction exists. So the acoustic dispersion and anisotropy might result in the abundant nature of refraction in arbitrary directions and will lead to some additional interesting effects as PCs, for example, acoustic collimating effects.

In addition, AANR (Ref. 12) is an important character for negative refraction and its application, which in acoustic waves was discussed in a three-dimensional sonic crystal of carbide beads in water[22] and a 2D system of water cylinders in mercury.[21] In the SC consisting of steel and air, calculated with the method described above, there is no AANR existing in our current crystal of $R=0.4a$ and the steel-in-air structure of $R=0.36a$ in Ref. 21. However, we found that AANR may appear at 41.2 kHz when R is greater than 1.05 mm ($R=0.42a$), and the frequency range of AANR is to be enlarged by increasing the filling fraction of steel cylinders. When $R=1.1$ mm ($R=0.44a$), it is from 38.1 to 40.1 kHz that AANR could be realized. So with the high filling fraction, AANR may also appear in the steel-in-air SC, which is very convenient to be used in applications.

To summarize, the acoustic single-beam negative refraction in the lowest band of 2D square SCs was theoretically analyzed by calculating the acoustic band structure and equifrequency surfaces and experimentally established in a 2D SC in the ultrasonic regime by scanning transmission measurements of spatial distributions of a single Gaussian beam. In order to obtain the larger negative refractive angle, it is necessary to make the bigger incident angle at the higher frequency. The acoustic negative refraction could be tuned to the desired frequency range by adjusting the lattice constant and constructing materials of the SC, for example, with immersing our structure into liquids such as water. In addition, acoustic negative refractions in our SC provide the possibilities to construct an acoustic superlens in air to realize both acoustic propagating and evanescent waves imaging.

The work was jointly supported by the National 863 High Technology Program, the State Key Program for Basic Research of China, and the National Nature Science Foundation of China (Grant No. 50225204).

*Electronic address: yfchen@nju.edu.cn

[1] V. G. Veselago, Sov. Phys. Usp. **10**, 509 (1968).
[2] J. B. Pendry *et al.*, Phys. Rev. Lett. **76**, 4773 (1996).
[3] J. B. Pendry *et al.*, J. Phys.: Condens. Matter **10**, 4785 (1998).
[4] J. B. Pendry *et al.*, IEEE Trans. Microwave Theory Tech. **47**, 2075 (1999).
[5] D. R. Smith *et al.*, 3Phys. Rev. Lett. **84**, 4184 (2000).
[6] R. A. Shelby *et al.*, Appl. Phys. Lett. **78**, 489 (2001).
[7] R. A. Shelby, D. R. Smith, and S. Schultz, Science **292**, 77 (2001).
[8] M. Notomi, Phys. Rev. B **62**, 10696 (2000).
[9] E. Cubukcu *et al.*, Nature (London) **423**, 604 (2003).
[10] B. Gralak, S. Enoch, and G. Tayeb, J. Opt. Soc. Am. A **17**, 1012 (2000).
[11] C. G. Parazzoli *et al.*, Phys. Rev. Lett. **90**, 107401 (2003).
[12] C. Luo *et al.*, Phys. Rev. B **65**, 201104(R) (2002).
[13] C. Luo, S. G. Johnson, and J. D. Joannopoulos, Appl. Phys. Lett. **81**, 2352 (2002).
[14] J. B. Pendry, Phys. Rev. Lett. **85**, 3966 (2000).
[15] A. A. Houck *et al.*, Phys. Rev. Lett. **90**, 137401 (2003).
[16] C. Luo *et al.*, Phys. Rev. B **68**, 045115 (2003).
[17] P. V. Parimi *et al.*, Nature (London) **426**, 404 (2003).
[18] E. Cubukcu *et al.*, Phys. Rev. Lett. **91**, 207401 (2003).
[19] X. Hu *et al.*, Phys. Rev. E **68**, 037301 (2003).
[20] X. Hu *et al.*, Phys. Rev. E **69**, 030201(R) (2004).
[21] X. Zhang and Z. Liu, Appl. Phys. Lett. **85**, 341 (2004).
[22] S. Yang, J. H. Page, Z. Liu, M. L. Cowan, C. T. Chan, and P. Sheng, Phys. Rev. Lett. **93**, 024301 (2004).
[23] E. Yablonovitch, Phys. Rev. Lett. **58**, 2059 (1987).
[24] S. John, Phys. Rev. Lett. **58**, 2486 (1987).
[25] J. D. Joannoupoulos, R. D. Meade, and J. N. Winn, *Photonic Crystals* (Princeton University Press, Princeton, NJ, 1995).
[26] E. N. Economou and M. Sigalas, J. Acoust. Soc. Am. **95**, 1734 (1994).
[27] F. Wu, Z. Liu, and Y. Liu, Phys. Rev. E **66**, 046628 (2002).
[28] M. Plihal and A. A. Maradudin, Phys. Rev. B **44**, 8565 (1991).